










Nuclear lamin isoforms differentially contribute to LINC complex-dependent nucleocytoskeletal coupling and whole-cell mechanics

Amir Vahabikashi^{a,1} , Suganya Sivagurunathan^a , Fiona Ann Sadsad Nicdao^a, Yu Long Han^b, Chan Young Park^c, Mark Kittisopikul^d , Xianrong Wong^e, Joseph R. Tran^f, Gregg G. Gundersen^g, Karen L. Reddy^h, G. W. Gant Luxtonⁱ , Ming Guo^b , Jeffrey J. Fredberg^c , Yixian Zheng^f, Stephen A. Adam^a , and Robert D. Goldman^{a,1}

Edited by Dennis Discher, University of Pennsylvania, Philadelphia, PA; received December 10, 2021; accepted March 18, 2022 by Editorial Board Member Yale E. Goldman

The ability of a cell to regulate its mechanical properties is central to its function. Emerging evidence suggests that interactions between the cell nucleus and cytoskeleton influence cell mechanics through poorly understood mechanisms. Here we conduct quantitative confocal imaging to show that the loss of A-type lamins tends to increase nuclear and cellular volume while the loss of B-type lamins behaves in the opposite manner. We use fluorescence recovery after photobleaching, atomic force microscopy, optical tweezer microrheology, and traction force microscopy to demonstrate that A-type lamins engage with both F-actin and vimentin intermediate filaments (VIFs) through the linker of nucleoskeleton and cytoskeleton (LINC) complexes to modulate cortical and cytoplasmic stiffness as well as cellular contractility in mouse embryonic fibroblasts (MEFs). In contrast, we show that B-type lamins predominantly interact with VIFs through LINC complexes to regulate cytoplasmic stiffness and contractility. We then propose a physical model mediated by the lamin–LINC complex that explains these distinct mechanical phenotypes (mechanophenotypes). To verify this model, we use dominant negative constructs and RNA interference to disrupt the LINC complexes that facilitate the interaction of the nucleus with the F-actin and VIF cytoskeletons and show that the loss of these elements results in mechanophenotypes like those observed in MEFs that lack A- or B-type lamin isoforms. Finally, we demonstrate that the loss of each lamin isoform softens the cell nucleus and enhances constricted cell migration but in turn increases migration-induced DNA damage. Together, our findings uncover distinctive roles for each of the four major lamin isoforms in maintaining nucleocytoskeletal interactions and cellular mechanics.

nuclear lamins | LINC complex | cell mechanics | cytoskeleton | mechanobiology

The ability of AQ9 mammalian cells to regulate their mechanical response to environmental forces is fundamental to their physiological functions and motile behavior. Cellular mechanics are facilitated by the complex cytoskeletal networks that extend from the nucleus to the cell periphery. The nucleus plays a significant role in cellular mechanics, as enucleated cells containing intact cytoskeletal systems exhibit altered mechanical properties and migratory behavior (1, 2). Hence, the interactions between the nucleus and the cytoskeleton are important for regulating cellular mechanics and motility.

The nuclear envelope (NE) is a specialized organelle that separates the nucleus from the cytoplasm and provides an interface for linking the genome to the various cytoplasmic cytoskeletal systems and the extracellular environment (3) (Fig. 1). The NE contains a double membrane that is a subdomain of the endoplasmic reticulum and the nuclear lamina (NL), which is a complex fibrillar meshwork of lamin intermediate filaments and their associated proteins that are closely juxtaposed to the nucleoplasmic face of the inner nuclear membrane. The lamin family is subdivided into either A-types (lamins A [LA] and C [LC]) or B-types (lamins B1 [LB1] and B2 [LB2]). LA and LC are alternatively spliced products of the *LMNA* gene that are expressed in most differentiated cell types, while the ubiquitously expressed LB1 and LB2 proteins are encoded by the *LMNB1* and *LMNB2* genes, respectively (3). Each lamin isoform assembles into a distinct meshwork, but the individual meshworks interact in ways that affect the structure of the other meshworks through unknown mechanisms (4).

The NL is physically coupled to the cytoskeleton through an NE-spanning molecular bridge known as the linker of nucleoskeleton and cytoskeleton (LINC) complex (5) (Fig. 1). Early studies in mouse embryonic fibroblasts (MEFs) showed that the deletion

Significance

Interactions between the cell nucleus and cytoskeleton regulate cell mechanics and are facilitated by the interplay between the nuclear lamina and linker of nucleoskeleton and cytoskeleton (LINC) complexes. To date, the specific contribution of the four lamin isoforms to nucleocytoskeletal connectivity and whole-cell mechanics remains unknown. We discover that A- and B-type lamins distinctively interact with LINC complexes that bind F-actin and vimentin filaments to differentially modulate cortical stiffness, cytoplasmic stiffness, and contractility of mouse embryonic fibroblasts (MEFs). We propose and experimentally verify an integrated lamin–LINC complex–cytoskeleton model that explains cellular mechanical phenotypes in lamin-deficient MEFs. Our findings uncover potential mechanisms for cellular defects in human laminopathies and many cancers associated with mutations or modifications in lamin isoforms.

The authors declare no competing interest.

This article is a PNAS Direct Submission. D.D. is a Guest Editor invited by the Editorial Board.

Copyright © 2022 the Author(s). Published by PNAS. This article is distributed under [Creative Commons Attribution-NonCommercial-NoDerivatives License 4.0 \(CC BY-NC-ND\)](https://creativecommons.org/licenses/by-nc-nd/4.0/).

¹To whom correspondence may be addressed. Email: amir.vahabikashi@northwestern.edu or r-goldman@northwestern.edu.

This article contains supporting information online at <http://www.pnas.org/lookup/suppl/doi:10.1073/pnas.2121816119/-/DCSupplemental>.

Published April 19, 2022.

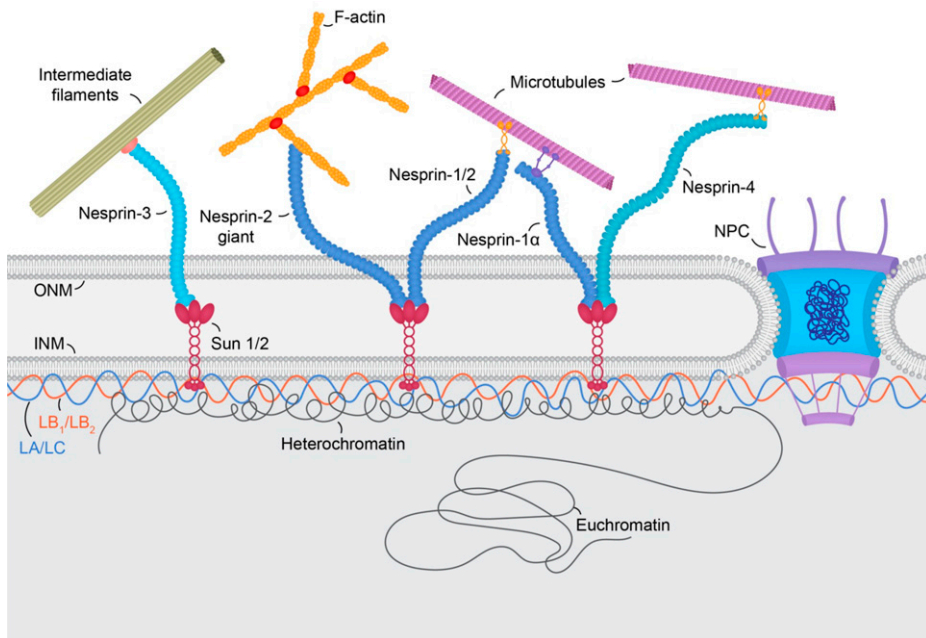


Fig. 1. Schematic illustration of the nuclear envelope in mammalian cells. The interplay between A-type (LA/LC) and B-type (LB1/LB2) lamins and LINC complexes at the nuclear envelope has been proposed to facilitate coupling of the nucleus to the cytoskeletal systems in the cytoplasm. Lamins further interact with peripheral heterochromatin to regulate chromatin organization within the cell nucleus (INM, inner nuclear membrane; NPC, nuclear pore complex; ONM, outer nuclear membrane).

of A-type or B-type lamins perturbs the organization of the perinuclear cytoskeleton and significantly softens the cell (6–8). However, the individual contributions from each of the four known nuclear lamin isoforms to cellular mechanics remain unknown.

Here, we conduct morphometric analyses to show that the loss of A-type lamin isoforms results in relatively larger nuclear and cellular volume in MEFs while the absence of B-type lamins tends to reduce the volume of the nucleus and the cell. We employ atomic force microscopy (AFM), optical tweezer (OT) microrheology, and traction force microscopy (TFM) to reveal that A-type lamins contribute to the stiffness of the cortex, the cytoplasm, and the contractile state whereas B-type lamins modulate cytoplasmic stiffness and the contractile state but not cortical stiffness. We then use fluorescence recovery after photobleaching (FRAP) to demonstrate that the differences in the mechanical phenotypes (mechanophenotypes) of A- and B-type lamin-deficient MEFs correlate with distinctive interactions of lamins with the LINC complexes that couple the nucleus to the F-actin and vimentin intermediate filament (VIF) cytoskeletons. We use these findings to introduce a model based on the lamin–LINC–cytoskeleton that explains the impaired cell mechanics incurred in the absence of each lamin isoform and experimentally verify the model by showing similar mechanophenotypes in MEFs with selectively disrupted LINC complexes. We further show that the loss of each lamin isoform compromises nuclear mechanics and that the resulting changes correlate with changes of the levels of heterochromatin. Finally, we show that the loss of either A- or B-type lamins increases the ability of MEFs to migrate in confined microenvironments accompanied by enhanced levels of migration-induced DNA damage. Together, our studies establish specific roles for each lamin isoform in maintaining nuclear and cellular morphology and mechanics.

Results

A- and B-type Lamins Affect Nuclear and Cellular Morphology in an Opposing Manner. Changes in the shape and volume of cells and their nuclei impact cellular mechanophenotypes

(9–11). Therefore, we investigated the effects of deleting specific lamin isoforms on nuclear and cellular morphology in MEFs using our previously described homozygous lamin knockout (KO) MEF lines LA-/LC- (here abbreviated as LA/C-), LB1-, and LB2-, as well as their wild type (WT) MEF controls (12). Since recent studies suggest that LA and LC perform distinct roles in establishing the cellular mechanophenotype (13–15), we also probed the specific contributions of these alternative splice variants in MEFs stably expressing short hairpin RNAs that knockdown (KD) either endogenous LA (LA KD) or LC (LC KD) (*SI Appendix, Fig. S1 A and B*).

Maximum projections and orthogonal sections of confocal images revealed significant nuclear shape changes in the lamin KO MEFs as compared to the WT MEFs (Fig. 2 *A* and *B*). WT MEF nuclei generally had an oblate spheroid profile with only a few surface distortions, while the profiles of nuclei in LA/C- MEFs were altered with an increased number of surface irregularities and distortions. In contrast, the LB1- and LB2-MEF nuclei appeared rounder than the WT MEF nuclei but lacked any readily observable distortions (Fig. 2 *A* and *B*). To quantify the distortions on the nuclear surface, we imported confocal z-sections of the nuclei to Imaris software to create 3-dimensional (3D) renderings and calculated the sum of squares for the distance between the nuclear surface and its center as a measure of nuclear surface roughness. The analysis showed a dramatic increase in the surface roughness of nuclei in LA/C- MEFs when compared to the nuclei in WT, LB1-, and LB2- MEFs (*SI Appendix, Fig. S2A*). In contrast, no differences between WT, LB1- and LB2- MEFs could be detected (*SI Appendix, Fig. S2A*). We next used the 3D renderings to analyze the sphericity of the nuclei. Nuclei in all the lamin KO or KD MEF lines were significantly rounder than those in the WT MEFs (Fig. 2 *C* and *SI Appendix, Fig. S2B*). To test whether re-expressing the depleted lamin isoform in its respective KO MEF rescued nuclear shape, we created MEF lines that stably expressed LA, LB1, or LB2 in the LA/C-, the LB1-, or the LB2- MEFs, respectively (*SI Appendix, Fig. S1 C and D*). We were unable to adequately rescue LC expression in LA/C- MEFs for these experiments, so those data are not included in our analyses. We found that the nuclei in all rescued KO

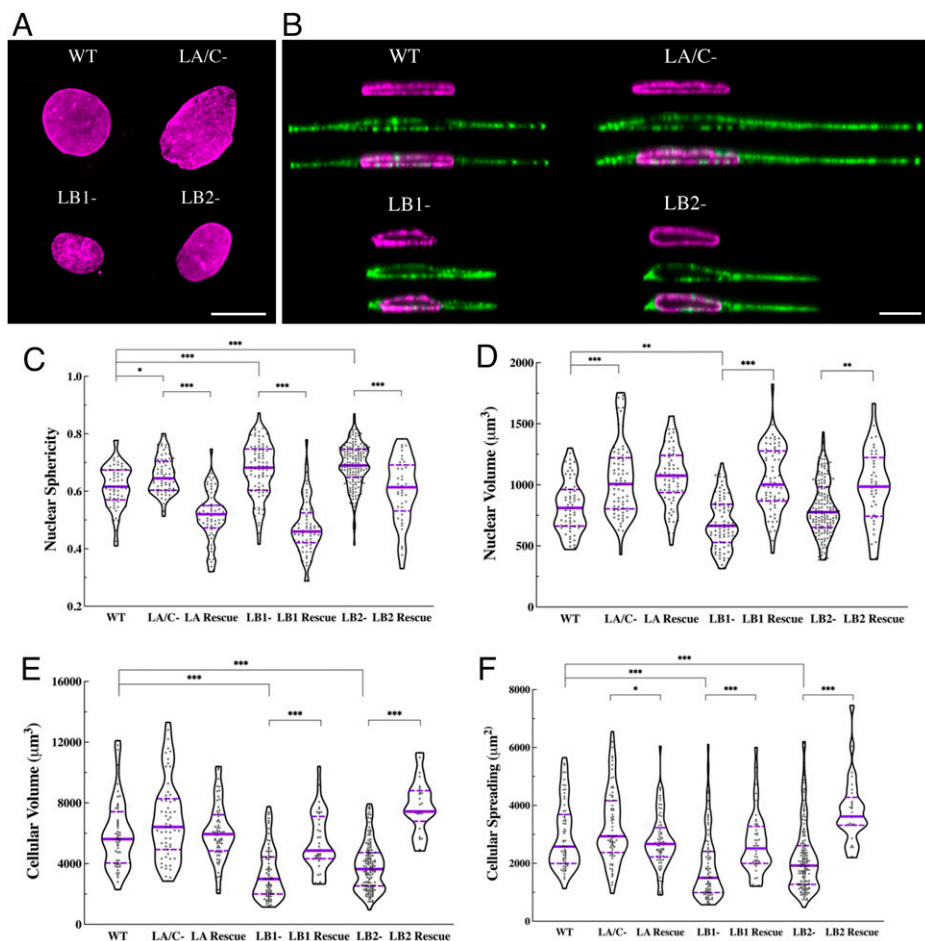


Fig. 2. Nuclear lamins are required for the maintenance of nuclear and cellular morphology. (A) Representative maximum projections of the nucleus and (B) orthogonal views of the nucleus (Top), F-actin (Middle), and their overlay (Bottom) in the indicated MEF lines stained for nuclear lamin (magenta) and F-actin (green). The nucleus in the WT, LA/C-, and LB2- MEF is stained with anti-LB1 and the nucleus in the LB1- MEF is stained with anti-LB2. Violin plots of the average (C) nuclear sphericity, (D) nuclear volume, (E) cellular volume, and (F) cellular spreading area in the WT (55 cells), lamin KO (59–135 cells), and rescued lamin KO MEFs (42–93 cells). For panels C–F, $n = 3$. The solid bars in the violin plots represent the median and the dashed lines mark the 25th and 75th percentiles (Scale bar, 20 μm). * $P < 0.05$, ** $P < 0.01$, *** $P < 0.001$.

MEF lines exhibited significant flattening toward the oblate profile observed in the WT MEFs (Fig. 2C).

Measurements of nuclear volume showed that relative to the WT MEFs, nuclei were significantly larger in the LA/C-, LA KD, and LC KD MEFs, smaller in the LB1- MEFs, and almost the same in the LB2- MEFs (Fig. 2D and *SI Appendix, Fig. S2C*). Rescue of LA expression in LA/C- MEFs was not sufficient to restore normal nuclear volume, suggesting a nonredundant role for LC in nuclear volume control (Fig. 2D). This observation contrasts with the re-expression of LB1 or LB2 in LB1- or LB2- MEFs, respectively, in which a significant increase in nuclear volume was noted (Fig. 2D).

In addition to the lamin isoform-dependent changes in nuclear shape and volume, we measured cellular volume using 3D confocal microscopy of cells stained with F-actin to mark the cell cortex (Fig. 2B). LA/C- MEFs had a slightly larger cellular volume than WT MEFs, whereas the cellular volumes of the LB1- MEFs and the LB2- MEFs were significantly reduced (Fig. 2E). LA KD in WT MEFs resulted in a significant increase in cellular volume, but LC KD showed a small but opposite effect on cellular volume that did not reach statistical significance (*SI Appendix, Fig. S2D*). Re-expressing the missing isoform tended to restore cellular volume to the levels observed in the WT MEFs by slightly decreasing it in the rescued LA/C- MEFs and significantly increasing it in the rescued LB1- and LB2- MEFs (Fig. 2E).

Previous studies suggest a relationship between the extent of cellular spreading and stiffness (10, 16). Therefore, we examined the effect of lamin isoform KO or KD on the cell spreading area. Our analyses showed that LA/C- MEFs spread slightly

more than WT MEFs, while LB1- and LB2- MEFs spread much less (Fig. 2F). Like the pattern observed for cellular volume, LA or LC KD had opposite effects on cell spreading: i.e., LA KD MEFs and LC KD MEFs displayed significantly increased and decreased cell spreading areas, respectively (*SI Appendix, Fig. S2E*). The cell spreading area of the rescued LA/C- MEFs was significantly decreased approaching WT levels, while both rescued LB1- and LB2- MEFs increased to WT levels or even greater (Fig. 2F).

Since nuclear and cellular volume tend to be positively correlated (17, 18), we determined the effect of lamin isoform expression on this relationship. Consistent with previous reports (18), linear regression analyses found a significant correlation between the nuclear and cellular volume in WT MEFs, lamin KO MEFs, and lamin KD MEFs (*SI Appendix, Fig. S2F and G*). However, the slopes of the regression lines calculated for LB1-, LB2-, and LC KD MEFs were significantly different from those calculated for WT, LA/C-, and LA KD MEFs (*SI Appendix, Fig. S2F and G*), suggesting that different modes of nucleocytoplasmic interactions may exist across these cell lines.

The size of the nucleus has also been positively correlated with an increase in cell size during cell cycle progression (19). To determine whether the differences in nuclear and cellular size related to lamin isoform expression may be biased by alterations in cell cycle distribution, we quantified the DNA content of each of the MEF lines using flow cytometry. The analyses showed insignificant differences in cell cycle distribution. Therefore, the differences in nuclear and cellular size of the various MEF lines are not due to the accumulation of cells at specific stages of the cell cycle (*SI Appendix, Fig. S3*).

Loss of A- or B-type Lamins Distinctively Compromises Cellular Mechanics.

The finding that MEFs with altered lamin composition exhibit changes in nuclear and cellular morphology suggests that both nuclear and whole-cell mechanics are also altered in these cells. To investigate this possibility, we developed a multipronged biophysical approach. Using AFM with large round probes (radius = 5 μm), we characterized the bulk stiffness of the cytoplasm as previously described (20). These measurements showed that the cytoplasm in all the lamin KO MEFs was significantly softer relative to the WT MEFs, with LB1- and LB2- MEFs being the softest (Fig. 3A). In addition, the depletion of LC significantly decreased the cytoplasmic stiffness, while the depletion of LA had a negligible effect (*SI Appendix, Fig. S4A*). Re-expressing LA in LA/C- MEFs or LB1 in LB1- MEFs stiffened the cytoplasm to levels observed in the WT MEFs (Fig. 3A). Rescuing the expression of LB2 in LB2- MEFs also increased the cytoplasmic stiffness of these cells, but not to the WT levels (Fig. 3A).

As a more direct measure of cytoplasmic stiffness, we used OT-based active microrheology (21). Our OT measurements were consistent with those obtained with the AFM round probe, demonstrating that LA/C- and LB1- MEFs had significantly softer cytoplasm compared to the WT MEFs and that LB2- MEFs exhibited a lesser reduction in the cytoplasmic stiffness (Fig. 3B). Furthermore, the cytoplasmic stiffness increased to WT levels upon rescuing the expression of the missing lamin isoforms in the corresponding lamin KO MEFs (Fig. 3B). Like the AFM measurements, the LC KD MEFs had a significantly softer cytoplasm while the LA KD MEFs exhibited a slight decrease in their cytoplasmic stiffness (*SI Appendix, Fig. S4B*).

Cell shape and spreading are known to associate with cortex stiffness (22,23). The relationships between lamin expression and cell spreading (see Fig. 2F) suggest that there may also be changes in the mechanical properties of the cell cortex in MEFs with altered lamin composition. We therefore used our previously established AFM method with a sharp pyramidal probe ($R = 20 \text{ nm}$) (20) to measure the apical cortex stiffness of the different MEF lines. The results revealed that the cortex of the LA/C- MEFs was significantly softer than the cortex of the WT MEFs, while cortical stiffness was mostly unaffected in the

LB1-, LB2-, LA KD, or LC KD MEFs (Fig. 3C and *SI Appendix, Fig. S4C*). We further found that rescuing the LA in LA/C- MEFs and LB1 in LB1- MEFs significantly stiffened the cortex (Fig. 3C), but no significant change in cortical stiffening was observed in LB2- MEFs rescued for the LB2.

The alterations in spreading area and cortex stiffness observed in the lamin KO and KD MEFs further suggested that the contractile forces exerted by these cells at their basal surfaces might also be lamin isoform-dependent. To determine whether this is the case, we used TFM in each MEF line to measure the strain energy (SE) and the net contractile moment (NCM) imparted by each cell to its substrate (24). The SE was notably reduced in all lamin KO and KD MEFs relative to the WT controls (Fig. 3D and *SI Appendix, Fig. S4D*). This phenomenon was reversed in rescue experiments as detected by the restoration of the WT levels of SE in the LA/C-, LB1-, and LB2- MEFs rescued for LA, LB1, and LB2, respectively (Fig. 3D). Further analyses of the NCM measurements showed a strong agreement with the results from the SE measurements, demonstrating a significant reduction of the contractile moment in LC KD MEFs as well as all lamin KO MEFs relative to the WT controls (*SI Appendix, Fig. S4E–F*). These reductions were restored to WT levels upon rescuing the expression of the missing lamin isoform (*SI Appendix, Fig. S4E*).

A- and B-type Lamins Distinctively Regulate the Dynamics of LINC Complexes that Bind F-actin and Vimentin.

We reasoned that the compromised cytoplasmic and cortical stiffness of the A- or B-type lamin KO MEFs might be related to defects in their ability to form proper nucleocytoskeletal connections via LINC complexes. Given the essential roles of the F-actin and VIF cytoskeletal systems in regulating cortical and cytoplasmic mechanics (20, 25, 26), we hypothesized that the assembly of LINC complexes that bind these cytoskeletal filaments might be defective in lamin KO MEFs.

To test this hypothesis, we first expressed enhanced green fluorescent protein (EGFP)-tagged mini-nesprin-2 giant (a previously characterized functional nesprin-2G construct [27]), EGFP-nesprin-3 α (28), EGFP-SUN1 (27), or EGFP-SUN2 (27) in the WT and lamin KO MEF lines. Nesprin-2G directly

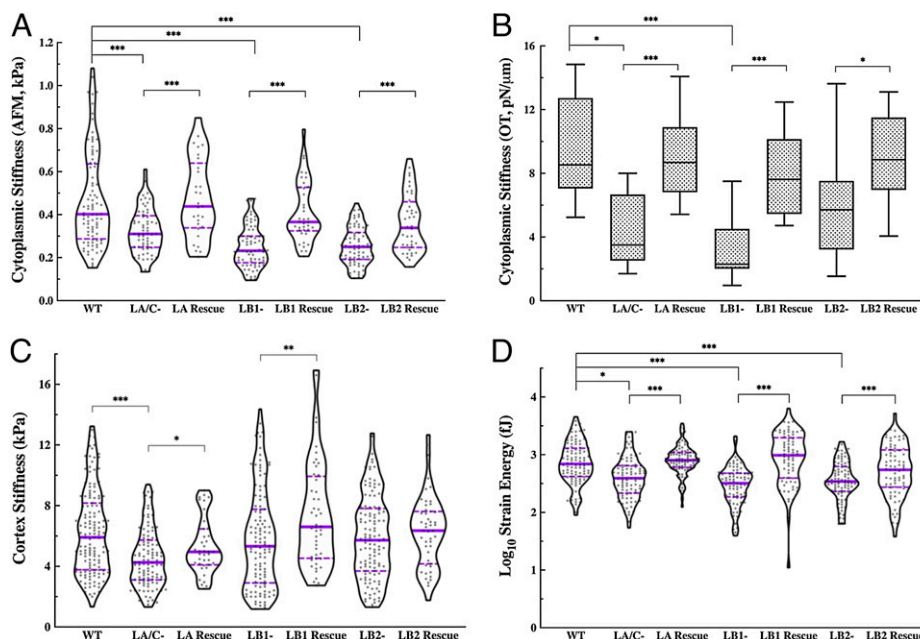


Fig. 3. The loss of A- and B-type lamins distinctively influence cellular mechanics. (A) Violin plots of the AFM round-probe measurements of the cytoplasmic stiffness in the WT ($n = 4$, 75 cells), lamin KO ($n = 4$, 69–75 cells), and rescued ($n = 4$, 30–40 cells) MEFs. (B) Box plots of OT measurements for the cytoplasmic stiffness in the WT ($n = 1$, 9 cells), lamin KO ($n = 1$, 9–13 cells), and rescued lamin KO ($n = 1$, 10–12 cells) MEFs. (C) Violin plots of the AFM sharp-probe measurements for the apical cortical stiffness in the WT ($n = 4$, 147 cells), lamin KO ($n = 4$, 117–130 cells), and rescued ($n = 4$, 44–50 cells) MEFs. (D) Violin plots of the logarithmically transformed SE in the WT ($n = 2$, 105 cells), lamin KO ($n = 2$, 80–94 cells), and rescued ($n = 2$, 82–98 cells) MEFs. The solid bars in the violin plots represent the median and the dashed lines mark the 25th and 75th percentiles. The bars and the whiskers in the box plots represent the median and the minimum/maximum, respectively. * $P < 0.05$, ** $P < 0.01$, *** $P < 0.001$.

interacts with F-actin (27, 29), while nesprin-3 α binds VIFs via plectin (30) (Fig. 1). Nesprin-2G and nesprin-3 α can both interact with SUN1 or SUN2 within the perinuclear space of the NE (31–33) (Fig. 1). Consistent with previous studies (28, 34), these EGFP-tagged proteins all localized to the NE in WT as well as lamin KO MEFs (*SI Appendix, Fig. S5A*).

To determine if the dynamic properties of the LINC complex proteins were disrupted when lamin isoform expression was altered, we carried out quantitative FRAP experiments in the NEs of the MEF lines that individually express each of the EGFP-tagged LINC complex proteins and determined the half-time ($t_{1/2}$) of recovery (*SI Appendix, Fig. S5B*). The fluorescence of EGFP-SUN1 and EGFP-SUN2 recovered in the NE bleached zone in all lamin KO MEFs (Fig. 4 *A* and *B*). However, the normalized $t_{1/2}$ for both EGFP-SUN1 and EGFP-SUN2 was significantly faster in the LA/C- and LB2- MEFs relative to the LB1- and WT MEFs (Fig. 4*E*). Furthermore, the fluorescence of EGFP-SUN2 in the LA/C- MEFs tended to recover significantly faster than in the NE of the LB2- MEFs (Fig. 4*E*). Therefore, the mobility of SUN1 and SUN2 is significantly increased in the LA/C- and LB2- MEFs as compared to the LB1- and WT MEFs.

FRAP analyses of EGFP-mini-nesprin-2G revealed a significantly faster recovery in the NE of the LA/C- MEFs (Fig. 4*C*),

but recovery rates in the LB1-, LB2-, and WT MEF NEs were indistinguishable (Fig. 4*E*). We further observed a dramatic increase in the normalized fluorescence intensity of EGFP-nesprin-3 α in all lamin KO MEFs (Fig. 4*D*), which manifested itself in a significantly faster normalized $t_{1/2}$ for EGFP-nesprin-3 α fluorescence recovery in the NEs of these cells (Fig. 4*E*). The data also suggested a relatively faster fluorescence recovery in the LA/C- and LB1- MEFs compared to the LB2- MEFs, although this difference was not statistically significant. These findings suggest that the loss of lamins increases the mobility of the F-actin- and VIF-binding LINC complexes within the NEs of the lamin KO MEFs. These observations are also consistent with previous studies that show the increased mobility of SUN1, SUN2, and nesprin-2G in the LA/C- MEFs (34–36). Taken together, the FRAP studies establish substantial and distinct roles for the A- and B-type lamins in regulating the mobility and, by extension, the assembly of LINC complexes that couple the nucleus to the F-actin or VIF cytoskeletons.

We next examined whether the increased mobility of LINC complex components in lamin-deficient MEFs affects the organization of either the F-actin or VIF cytoskeletal systems, particularly in the perinuclear region. We used confocal imaging to investigate and quantitate the formation of F-actin stress fibers above the nucleus, referred to as F-actin

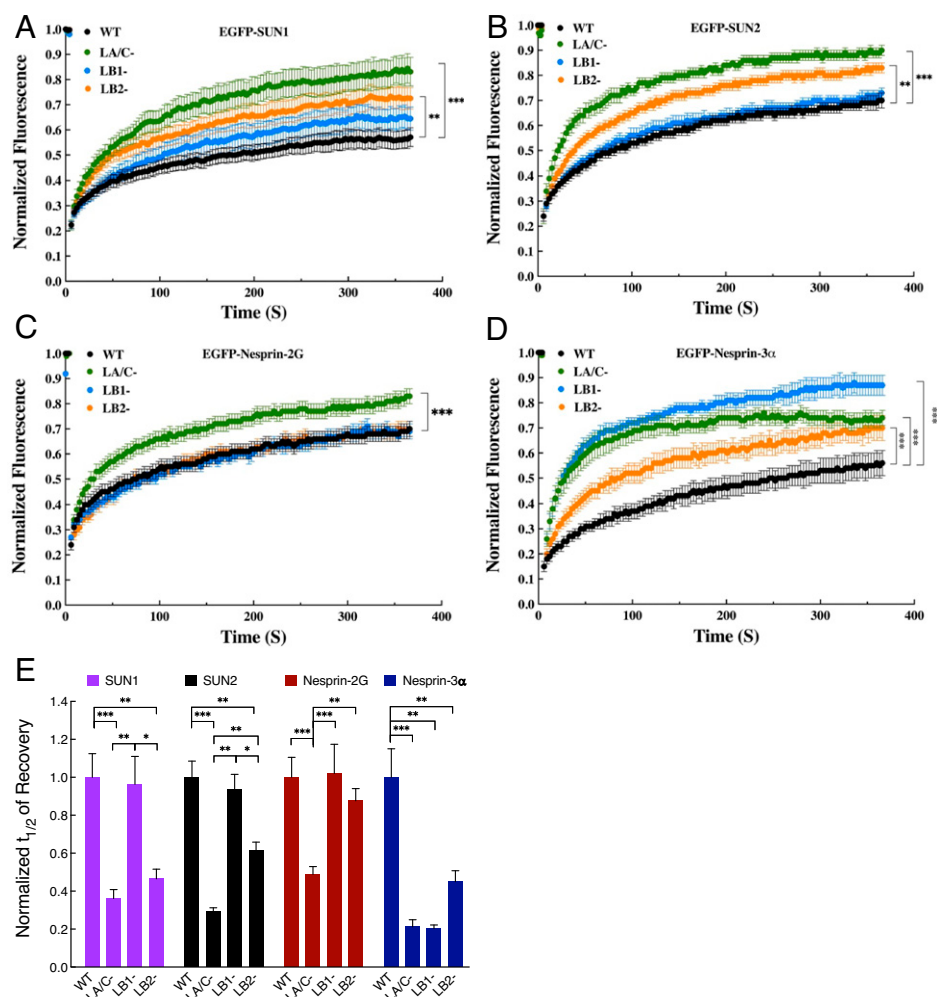


Fig. 4. A- and B-type lamins distinctively regulate the dynamics of F-actin or vimentin-binding LINC complex components at the NEs of the MEFs. Plots of the normalized fluorescence recovery of (A) EGFP-SUN1, (B) EGFP-SUN2, (C) EGFP-mini-nesprin-2G, and (D) EGFP-nesprin-3 α in the NEs of the WT, LA/C-, LB1-, and LB2- MEF lines. (E) Bar plots of the normalized $t_{1/2}$ of NE FRAP for the indicated EGFP-tagged LINC complex constructs expressed in the WT, LA/C-, LB1-, and LB2- MEF lines. The reported values are normalized to those obtained in the WT MEFs. See *SI Appendix, Fig. S5B* for the absolute numbers of $t_{1/2}$. Data are shown as mean \pm SE ($n \geq 2$; 10–15 cells per experimental condition). * $P < 0.05$, ** $P < 0.01$, *** $P < 0.001$.

caps (*SI Appendix, Fig. S6 A and B*) (37, 38). The results showed that between 65 and 80% of WT and lamin KO MEFs contain F-actin caps and that there are no statistically significant differences among the cells assayed (*SI Appendix, Fig. S6B*). We further found that VIFs consistently formed a perinuclear cage-like structure surrounding the bottom and top surfaces of the nuclei in all examined MEFs (*SI Appendix, Fig. S6A*). However, closer examination of the VIF distribution indicated the loss or disruption of perinuclear VIF cages in lamin KO MEFs, which were notably restored upon rescuing the missing lamin isoform in these cells (*Fig. 5A*). We further employed circular variance analyses to investigate the uniformity of perinuclear VIF distribution within 2 μm of the nuclear surface. The results demonstrated that the distribution of perinuclear VIFs in LA/C- and LB2- MEFs are significantly less uniform when compared to WT and LB1- MEFs. This altered distribution becomes more uniform and similar to WT controls following the rescue of LA and LB2 in LA/C- and LB2- MEFs (*Fig. 5B*). Furthermore, observations of orthogonal sections of WT and lamin KO MEFs showed that VIFs colocalize with F-actin at both the basal and apical cell cortices (*SI Appendix, Fig. S6C*) (20, 39).

Inhibition or Depletion of the LINC Complex Components Replicates the Mechanical Defects Caused by Lamin KO. The FRAP results suggest relationships between the lamins, cellular stiffness, and the ability of cells to assemble functional LINC complexes. Therefore, we hypothesized that inhibiting the function of LINC complex components should result in cellular mechanophenotypes like those observed in the lamin KO MEFs. To test this hypothesis, we used AFM to measure cortical and cytoplasmic stiffness in MEFs expressing signal sequence (SS)-EGFP-tagged dominant negative LINC complex constructs that disrupt LINC connections to the cytoskeleton: SS-EGFP-KASH2, SS-EGFP-KASH4, and SS-EGFP-SUN1^{LD} (40). Controls consisted of SS-EGFP-KASH2^{ΔPPPT} for SS-EGFP-KASH2 and -KASH4 and SS-EGFP-KDEL for SS-EGFP-SUN1^{LD} (40). We also used nontransfected WT MEFs as a second control for these dominant negative construct expression experiments. Immunofluorescence demonstrated that the expression of each of the three dominant negative constructs in WT MEFs displaced endogenous nesprin-2G from the NE to the endoplasmic reticulum within 24 h after transfection (*SI Appendix, Fig. S7A*), consistent with their ability to inhibit the LINC complex assembly

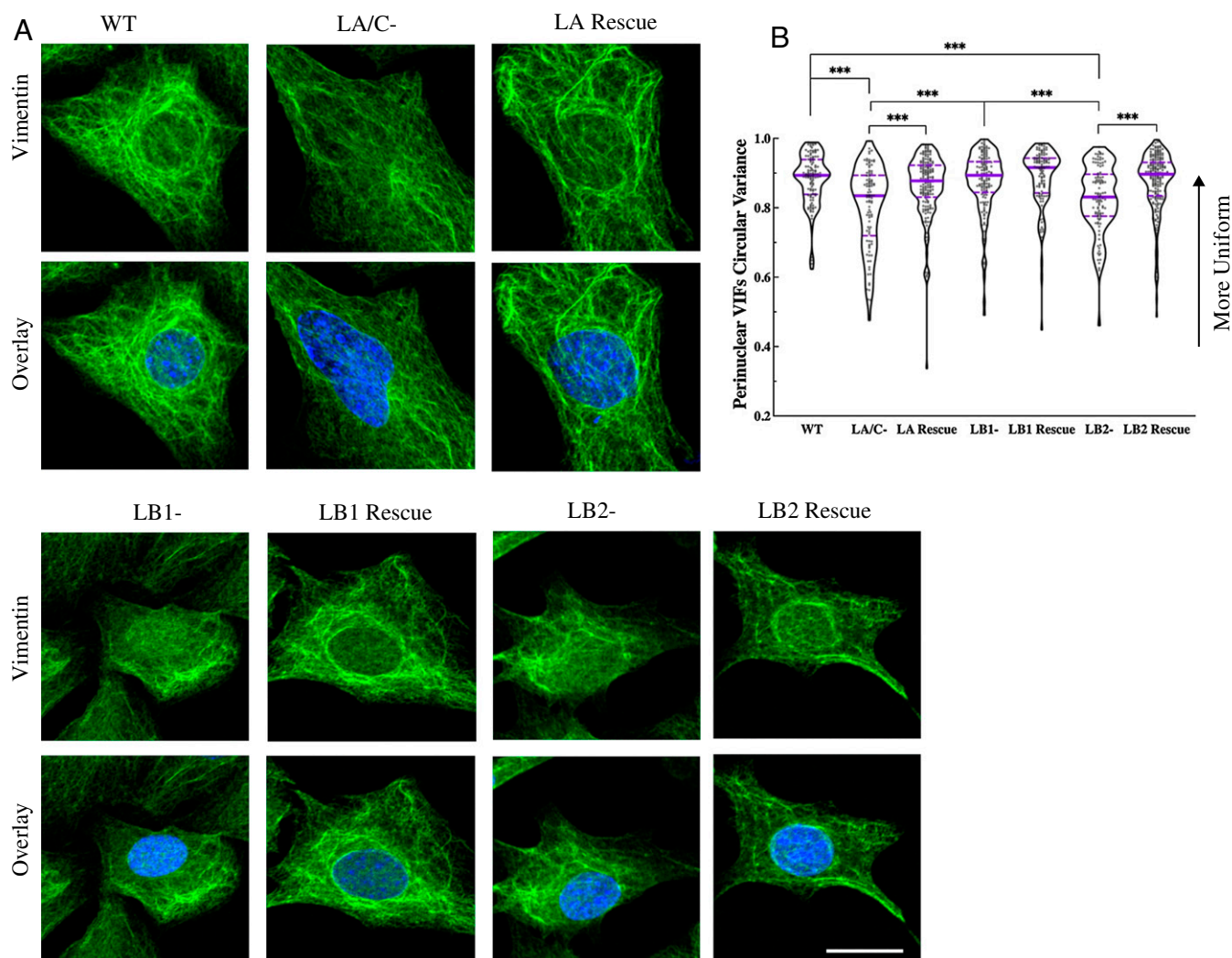


Fig. 5. Disrupted distribution of VIFs in lamin-deficient MEFs. (A) Representative images of the nucleus (blue) and VIF (green) distribution in WT and lamin KO MEFs and their corresponding rescue lines shown as maximum projections of confocal stacks. These images demonstrate the loss or disruption of the perinuclear VIF cages and the translocation of VIFs away from the nucleus in lamin KO MEFs and the restoration of a more uniform perinuclear distribution upon rescuing the missing lamin isoform. (B) Circular variance for perinuclear VIFs in WT ($n = 2, 112$ cells), lamin KO ($n = 2, 98\text{--}140$ cells), and rescued MEFs ($n = 2, 108\text{--}198$ cells). The solid bars in the violin plots represent the median and the dashed lines mark the 25th and 75th percentiles (Scale bar, 20 μm). *** $P < 0.001$.

(41, 42). Therefore, the AFM measurements for dominant negatives were carried out 24 h post transfection.

AFM round-tip measurements demonstrated that the expression of SS-EGFP-KASH2 or SS-EGFP-KASH4 significantly softened the cytoplasm of WT MEFs when compared to nontransfected MEFs or MEFs expressing the SS-EGFP-KASH2^{ΔPPPT} control construct (Fig. 6A). Similarly, the expression of SS-EGFP-SUN1^{LD} resulted in a significantly softer cytoplasm in WT MEFs when compared to nontransfected WT MEFs or those expressing the SS-EGFP-KDEL control construct (Fig. 6A). Cortical stiffness measurements with AFM sharp-tip probes showed that the expression of SS-EGFP-KASH2 resulted in a significant softening of the cell cortex in WT MEFs compared to nontransfected controls and a notable yet statistically insignificant softening compared to the

WT MEFs expressing the SS-EGFP-KASH2^{ΔPPPT} control construct (Fig. 6B). The cortex was also significantly softer in WT MEFs expressing either SS-EGFP-KASH4 or SS-EGFP-SUN1^{LD}, as compared to nontransfected WT MEFs or those expressing the appropriate corresponding controls (Fig. 6B).

Having established a role for the LINC complex in regulating both cortical and cytoplasmic stiffness in WT MEFs, we next reasoned that if lamins were regulators of cellular mechanics through their physical interactions with LINC complexes, then the depletion of LINC complex components that bind the F-actin or VIF cytoskeletons should have minimal or no additional effects on the mechanics of the lamin KO MEFs, since the nucleocytoskeletal coupling would be impaired at the site of attachment to the lamina in these cells. To test this

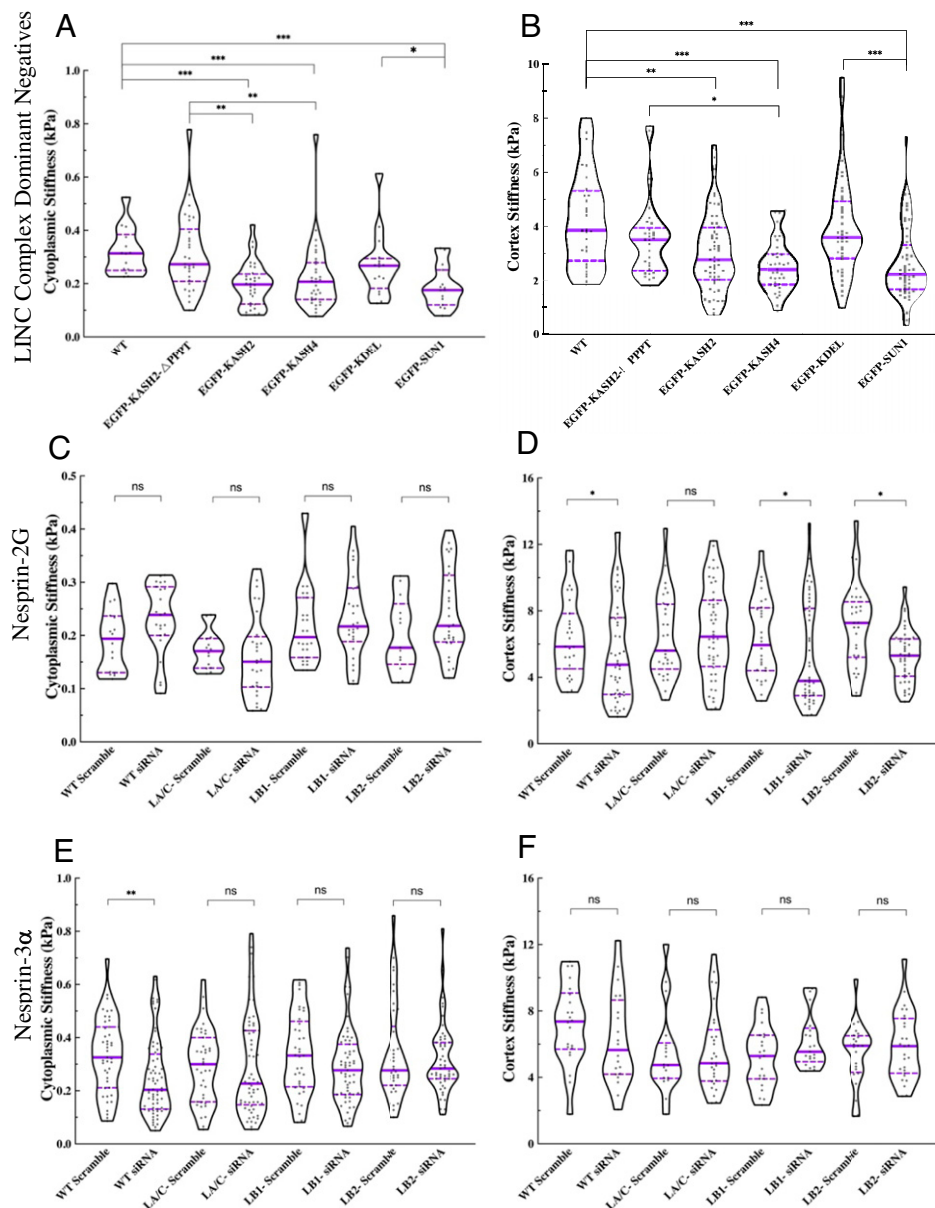


Fig. 6. LINC complex inhibition and depletion of nesprin-2G or nesprin-3 α recapitulates the cellular mechanophenotypes caused by the absence of the nuclear lamins in MEFs. Violin plots of the (A) cytoplasmic and (B) cortical stiffness measurements in nontransfected WT MEFs and upon the expression of the indicated SS-EGFP-tagged dominant negative LINC complex inhibitor constructs or their corresponding controls (at least 15 cells measured per experiment). Violin plots of the (C) cytoplasmic and (D) cortical stiffness measurements in the WT, LA/C-, LB1-, and LB2- MEFs treated with either the noncoding control or the nesprin-2 siRNA ($n = 2$, at least 15 cells measured per experiment). Violin plots of the (E) cytoplasmic and (F) cortical stiffness measurements in the WT, LA/C-, LB1-, and LB2- MEFs treated with either the noncoding control or the nesprin-3 α siRNA ($n = 2$, at least 15 cells per experiment). The solid bars in the violin plots represent the median and the dashed lines mark the 25th and 75th percentiles. * $P < 0.05$, ** $P < 0.01$, *** $P < 0.001$.

possibility, we depleted endogenous nesprin-2G or nesprin-3 α in WT and lamin KO MEFs by treating them with small interfering RNAs (siRNAs) for 48 h (*SI Appendix, Fig. S7B*) and then performed AFM measurements in these cell lines. For controls, we performed AFM measurements in WT and lamin KO MEFs treated with scrambled siRNAs. The depletion of nesprin-2G had a slight effect on the stiffness of the cytoplasm in WT MEFs, but none of the changes were statistically different from those measured in WT MEFs treated with the control siRNAs (Fig. 6C). However, nesprin-2G depletion significantly softened the cortex in WT, LB1-, and LB2- MEFs but had a negligible effect on the cortical stiffness of LA/C- MEFs (Fig. 6D). We further found that the depletion of nesprin-3 α from WT MEFs resulted in a significantly softer cytoplasm, but it did not change cytoplasmic stiffness in any of the lamin KO MEFs (Fig. 6E). In addition, cortical stiffness was slightly reduced in nesprin-3 α -depleted WT MEFs, and no detectable changes in cortical stiffness were observed in any of the nesprin-3 α -depleted lamin KO MEFs (Fig. 6F). Taken together, these results demonstrate that the A-type lamin isoforms interact with F-actin and VIF-binding LINC complexes to regulate the mechanical properties of the cell cortex and cytoplasm whereas B-type lamins engage with VIF-binding LINC complexes to modulate the stiffness of the cytoplasm.

Loss of A- or B-type Lamins Compromises Nuclear Stiffness and Alters Heterochromatin Levels. Lamins are proposed to regulate nuclear mechanics not only through their nonlinear mechanical properties as intermediate filament polymers but also through their influence on the organizational state of chromatin (e.g., euchromatin vs. heterochromatin) (43–47). However, the individual contribution of each lamin isoform to nuclear stiffness is incompletely understood. To begin to address this knowledge gap, we measured the bulk stiffness of the nucleus in the lamin KO, KD, and rescued MEF lines using AFM with large round tips ($R = 5 \mu\text{m}$) to indent over the center of the nucleus as described previously (48, 49). The nuclei in all lamin KO MEFs were significantly softer than the nuclei in the WT MEFs, with the degree of softening comparable between the lamin KO lines (*SI Appendix, Fig. S8A*). However, we observed that nuclear stiffness did not change in either LA KD or LC KD MEFs relative to the WT MEFs (*SI Appendix, Fig. S8B*). Re-expressing LA in the LA/C- MEFs dramatically stiffened the nucleus to levels that were even greater than those observed in the WT MEFs (*SI Appendix, Fig. S8A*). Nuclear stiffness in the rescued LB1- MEFs was restored to the same level as was detected in WT MEFs (*SI Appendix, Fig. S8A*). However, this was not the case for the rescued LB2- MEFs, where the nucleus became slightly stiffer but not to the same extent as observed in the WT MEFs (*SI Appendix, Fig. S8A*).

We also used OT to measure nuclear stiffness more directly in the MEF lines by locating endocytosed latex beads ($R = 0.25 \mu\text{m}$) in the cytoplasm adjacent to the nucleus and dragging them toward the nucleus to indent the nuclear surface (50). Similar to our AFM results, the OT measurements showed a significant decrease in nuclear stiffness in LA/C- and LB1- MEFs relative to the WT MEFs (*SI Appendix, Fig. S8C*). In addition, a notable yet statistically insignificant decrease in nuclear stiffness was measured in LB2- MEFs compared to the WT MEFs (*SI Appendix, Fig. S8C*). Nuclear stiffness measurements performed in all rescued lamin KO MEFs also revealed a notable but statistically insignificant increase in nuclear stiffness relative to the WT MEFs (*SI Appendix, Fig. S8C*). In contrast

to our AFM studies, the OT measurements indicated that LA KD significantly softened the nucleus, whereas LC KD had a marginal effect on the nuclear stiffness (*SI Appendix, Fig. S8D*).

It has been shown that heterochromatin regulates small mechanical deformations of the nucleus (43). Given the small deformations ($< 1 \mu\text{m}$) inherent in the AFM and OT assays, we speculated that the observed decreases in nuclear stiffness in the lamin KO and KD MEFs may be, at least in part, related to changes in their levels of the heterochromatic markers H3K9me2, H3K9me3, and H3K27me3, which have been shown to be associated with nuclear stiffness (15, 44, 51). Therefore, we determined the levels of these heterochromatic markers in lamin KO and KD MEFs using quantitative immunofluorescence and Western blot analyses (*SI Appendix, Fig. S8E–H*).

Quantification of the mean fluorescence intensity for H3K9me2 showed a significant increase in LA/C- MEFs relative to the WT controls, but the fluorescence intensity levels in LB1-, LB2-, LA KD, and LC KD MEFs remained unchanged (*SI Appendix, Fig. S8F*). In addition, the mean fluorescence intensities of H3K9me3 were significantly reduced in LA/C- and LB2- MEFs, as compared to the WT and LB1- MEFs (*SI Appendix, Fig. S8G*). Furthermore, the mean fluorescence intensity of H3K9me3 was also significantly reduced in LC KD MEFs relative to the WT and LA KD MEFs (*SI Appendix, Fig. S8G*).

The mean fluorescence intensity of H3K27me3 was dramatically reduced in all lamin KO MEFs relative to the WT MEFs (*SI Appendix, Fig. S8H*). However, the extent of this decrease was different between the lamin KO MEFs, with LB1- MEFs showing significantly lower intensity compared to the LA/C- and LB2- MEFs, and LA/C- MEFs demonstrating lower intensity relative to the LB2- MEFs. The LA KD MEFs exhibited increased H3K27me3 intensity relative to the WT MEFs, while the fluorescence intensity in the LC KD MEFs was similar to that of the WT MEFs (*SI Appendix, Fig. S8H*). To further verify the results from the immunofluorescence studies, we examined the expression levels of H3K9me and H3K27me in the WT, lamin KO, and lamin KD MEFs through Western blot analysis (*SI Appendix, Fig. S8I*). Data from the Western blots showed good agreement with the immunofluorescence results, suggesting an overall decrease in the level of these heterochromatic markers in the lamin KO and KD MEFs. Together, these results show that the loss of each lamin isoform reduces heterochromatin levels, which in turn may contribute to nuclear softening.

Loss of A- and B-type Lamin Isoforms Alters Cell Motility and Increases DNA Damage Caused by Constricted Cell Migration.

Loss or altered expression levels of A- and B-type lamins have been associated with changes in cell migration (6, 52–54). Therefore, we studied the relationship between the altered cellular mechanics observed in lamin KO and KD MEFs and their motility in 2-dimensional (2D) and 3D-like environments. In a 2D wound healing assay (*SI Appendix, Fig. S9A*), LA/C- MEFs migrated at marginally higher rates than WT MEFs, whereas LB1- and LB2- MEFs moved at significantly higher rates (*SI Appendix, Fig. S9B*). In addition, LA KD MEFs and LC KD MEFs migrated slower and faster than WT MEFs, respectively (*SI Appendix, Fig. S9C*). To examine the relationships between lamin isoforms and cell migration in 3D-like microenvironments, we used transwell migration assays with either 3 or 5 μm pore diameters to induce two levels of mechanical stress. When migrating through the 5 μm pores, LA/C- and LB2- MEFs, but not LB1- MEFs, migrated at significantly higher levels relative to WT MEFs (*SI Appendix, Fig. S9D*). The overall migration of these MEF lines through the 3 μm pores was

generally reduced, but the average migration ability was significantly increased in all lamin KO MEFs when compared with the WT MEFs (SI Appendix, Fig. S9D). The migration of LA KD and LC KD MEFs across both the 3 and 5 μm pore diameters was comparable to that observed with WT MEFs (SI Appendix, Fig. S9E). To examine the role of nuclear size in cell migration through the pores, we compared our migration data to the average diameter of the nuclei normalized by the pore diameter (SI Appendix, Fig. S9 F and G). The results suggest that despite comparable ratios for the nuclear-to-pore diameter, cell migration rates were significantly higher in lamin KO MEFs relative to the WT MEFs.

We next attempted to rescue the migratory behavior of the lamin KO MEFs by exogenously expressing the missing lamins in these cells and examining their ability to migrate through 3 μm pores. The migration of rescued LA/C- and rescued LB1-MEFs through 3 μm pores was indistinguishable from the WT MEFs (SI Appendix, Fig. S9H). The migration of rescued LB2-MEFs was slightly decreased but was still significantly higher relative to the WT MEFs (SI Appendix, Fig. S9H). We also observed that for all examined MEF lines, the average nuclear area of the cells that migrated through the pores was smaller than the nuclear area of those that remained at the top of the transwell (SI Appendix, Fig. S9 I and J). This finding is consistent with previous studies showing that smaller pores select for cells with smaller nuclei (18, 55).

Cell migration through constricted spaces is associated with an accumulation of damaged DNA within the nucleus (18, 56–58). Therefore, we stained transwell membranes with γ -H2AX (SI Appendix, Fig. S10A) to detect double-strand DNA breaks (59) to determine whether the loss of lamin isoforms affects migration-induced DNA damage in lamin KO and KD MEFs. The normalized counts for γ -H2AX foci per nucleus was compared between cells that migrated and did not migrate through the pores. The results showed that LA/C- and LB2- MEFs exhibited a more than 50% and 70% increase in γ -H2AX foci compared to WT MEFs, respectively (SI

Appendix, Fig. S10B). DNA damage was also increased by more than 20% in LB1-, LA KD, and LC KD MEFs relative to WT MEFs, but these increases were not statistically significant (SI Appendix, Figs. S10 B and C).

Discussion

Our results demonstrate that all four major lamin isoforms contribute to mammalian cell mechanics and suggest that this contribution is mediated by a selective lamina–LINC complex–cytoskeleton mechanism (Fig. 7). Specifically, we found that A-type lamins engage with nesprin-2G- and nesprin-3 α -containing LINC complexes, and therefore F-actin and VIFs, to respectively modulate the cortical and cytoplasmic stiffness of the MEFs, while B-type lamins harness nesprin-3 α and VIFs to regulate cytoplasmic stiffness but not cortical stiffness (Fig. 7 B–E). We further showed that each lamin isoform is involved in regulating the contractile properties of MEFs through their interactions with the F-actin and VIF cytoskeletons. These findings extend the functional reach of the nuclear lamins well beyond their established roles as key determinants of nuclear stiffness to more global regulators of the elastic, contractile, and migratory properties of the whole cell.

We employed both AFM nanoindentation analyses and OT microrheology measurements to characterize the effect of each lamin isoform on cytoplasmic mechanics. The OT uses the motion of a small bead ($R = 0.25 \mu\text{m}$) to locally characterize the stiffness of the cytoplasm, whereas our previous studies using finite element modeling demonstrated that spherical AFM tips ($R = 5 \mu\text{m}$) measure the bulk stiffness of the cytoplasm because of the large size of the indenting probe (20, 25, 60). Here, we showed that the cytoplasm is much softer in the LA/C-, LB1-, and LB2- MEFs relative to the WT MEFs. Our studies confirm earlier findings on softened cytoplasm in LA/C-MEFs (6–8) and further reveal that the cytoplasm is also notably softer in both LB1- and LB2- MEFs. We also discovered that the depletion of endogenous LC but not LA compromises cytoplasmic stiffness in MEFs. This result is further supported

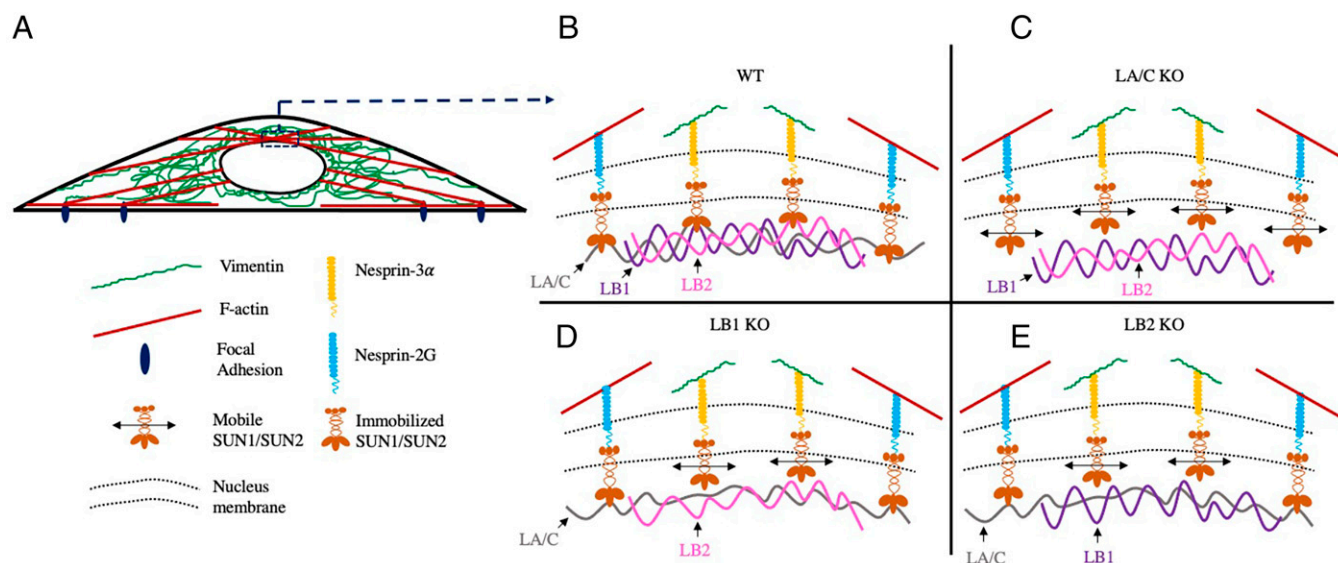


Fig. 7. The proposed lamina–LINC complex–cytoskeleton model for the regulation of cellular mechanics. (A) The nuclear lamina interacts with F-actin connecting the apical cortex to focal adhesions (FAs) and a perinuclear cage of VIFs that extends to the plasma membrane where VIFs interact with F-actin and FAs. (B) LA/C, LB1, and LB2 immobilize the LINC complex proteins SUN1, SUN2, nesprin-2G, and nesprin-3 α at the nuclear envelope, enabling them to efficiently bind F-actin and VIFs and consequently regulate cortex stiffness, cytoplasmic stiffness, and cellular contractility. (C) Loss of LA/C increases the mobility of nesprin-2G and nesprin-3 α -interacting LINC complexes, impairing the coupling of the nucleus with F-actin and VIFs, thus resulting in a softer cortex and cytoplasm as well as lower cellular contractility. (D) Loss of LB1 or (E) LB2 increases the mobility of nesprin-3 α -interacting LINC complexes, resulting in defective connections between the nucleus and VIFs and thereby a softer cytoplasm and lower contractility.

by the finding that LC expression levels correlate with the mechanical properties of the whole cell (14). The strong agreement between our OT and AFM round-probe measurements suggests that the loss of specific lamin isoforms softens the cytoplasm at both the local and global scales. We hypothesize that this effect could be due to dysfunctional nucleocytoplasmic connections with the VIF cytoskeleton, since it is a key determinant of cytoplasmic stiffness (20, 21, 25, 61). Support for this hypothesis comes from our FRAP results for EGFP-nesprin-3 α that revealed highly destabilized nuclear connections to VIFs via LINC complexes in lamin KO MEFs, accompanied by disruptions in the perinuclear cage of the VIFs. Our nesprin-3 depletion experiments also showed that disrupting the LINC complexes coupling VIFs to the nucleus significantly softens the cytoplasm in WT MEFs but not in lamin KO MEFs. These findings, along with the data from the rescue experiments, which demonstrate the restoration of cytoplasmic stiffness and perinuclear VIF distribution, suggest that the LA/C, LB1, and LB2 meshworks interact, directly or indirectly, with LINC complexes to mediate the coupling of the nucleus to the VIF cytoskeleton (Fig. 7 A–E). Such interactions are further supported by the finding that the removal of any single lamin isoform is sufficient to disrupt this connection and, consequently, compromise cytoplasmic stiffness.

Our AFM sharp-tip measurements reveal that the loss of LA/C, but not LB1 or LB2, significantly softens the cell cortex in MEFs, demonstrating the importance of understanding the different roles played by each lamin isoform in regulating the mechanical properties of the entire cell. Previous studies of LA/C- MEFs have documented impaired nesprin-2G-mediated anchorage of transmembrane actin-associated nuclear lines to the nucleus (27), loss or disruption of contractile F-actin caps at the dorsal nuclear surface (38), and deregulation of actomyosin remodeling (62). These alterations in the actomyosin cytoskeleton agree with our findings and those of others showing an increased mobility of nesprin-2G in the NE of LA/C- MEFs (34). In contrast, we show that the loss of B-type lamins does not change the mobility of nesprin-2G within the NE and that there is no significant effect on the stiffness of the apical cortex. Since we did not find any differences in either perinuclear F-actin cap formation or the overall distribution of cortical F-actin between WT and lamin KO MEFs, it is likely that the dynamic coupling of these contractile fibers to the dorsal surface of the nucleus, which is mediated by nesprin-2G-LA/C, modulates the stiffness of the apical cortex (Fig. 7 A–E). This proposed model (Fig. 7) is supported by our siRNA experiments showing that nesprin-2G depletion dramatically softens the apical cortex in WT, LB1-, and LB2- MEFs but not in LA/C- MEFs. Further live cell imaging studies of the perinuclear F-actin could shed light on the potentially altered dynamics of F-actin binding to the nucleus in lamin KO MEFs. We further show that the depletion of either LA or LC has no effect on cortical stiffness and that restoring the expression of LA in LA/C- MEFs significantly stiffens the cell cortex. These findings suggest that either LA or LC is likely sufficient to properly immobilize nesprin-2G at the NE. Our results also show that while the loss of LB1 in LB1- MEFs results in an insignificant drop in cortical stiffness, rescuing LB1 in these cells significantly stiffens their cortex. This may be due to the effect of LB1 expression on the LA/C filamentous meshwork, where LB1- MEFs, but not LB2- MEFs, contain a substantially enlarged LA/C mesh size relative to the LA/C meshwork in WT MEFs (4, 63). In other words, it is likely that in addition to the composition of the nuclear lamina, the organization of

its meshwork could likely modulate cytoskeletal dynamics and cell stiffness.

Our results also reveal a correlation between the loss of contractility in lamin KO and KD MEFs and alterations in the LINC complex dynamics within their NEs. Recent models suggest that the magnitude of cellular traction forces is regulated by cross talk between the nucleoskeleton- and cytoskeleton-generated tensions and their interactions with focal adhesions (1, 64). The restoration of contractility to the WT level upon the re-expression of missing lamin isoforms described in this study further supports the central role of lamins in the nucleocytoplasmic cross talk regulating cell contractility and motility. It is conceivable that nesprin-2G-mediated coupling of the nucleus and the actomyosin cytoskeleton would influence cellular contractility (64). However, our results show that both LB1- and LB2- MEFs exhibit significantly reduced cellular contractility, which is restored in rescue experiments. These findings suggest that the nesprin-3 α -mediated nucleocytoplasmic connection to VIFs also significantly contributes to regulating traction forces. We suggest that VIFs fulfill this role through interacting with contractile F-actin and focal adhesions (Fig. 7A). In support of this idea, it has been shown that VIFs can interact with stress fibers (39, 65, 66), govern the alignment of actin-based traction forces (67), and also regulate and associate with focal adhesions (68, 69). In fact, MEFs that are devoid of VIFs are significantly less contractile (by more than 30%) when compared to WT MEFs (20).

The loss of lamins is associated with altered nuclear shape and mechanics (47, 54, 70). Originally, LA/C was proposed as the dominant lamin isoform regulating nuclear stiffness (70). However, our findings and those of others have shown that both LB1 and LB2 also contribute to nuclear stiffness (45, 71). The AFM and OT indentations made in our studies cause small deformations in the nucleus ($< 1 \mu\text{m}$), a deformation regime that is predominantly determined by heterochromatin (43). We found that the significant softening of nuclei detected in the lamin KO MEFs correlates with reduced levels of their heterochromatic markers, H3K9me3 and H3K27me3, both known to regulate the mechanical properties of the nucleus (44, 51).

Our results showing that lamin KO MEFs move faster than WT MEFs in transwell migration assays are consistent with the notion that nuclear stiffness is a physical limit for confined cell migration (72). The reduction in migration through $3 \mu\text{m}$ detected in the lamin KO rescue experiments lends further support to the proposal that enhanced nuclear stiffness reduces the migratory behavior of MEFs. The increased migratory activity of lamin KO MEFs is accompanied by significant increases in the levels of confined migration-induced double-stranded DNA damage. These results agree with previous reports showing a relationship between increased deformability and double-stranded DNA damage observed in cells with softer nuclei post-migration (52, 73).

In summary, our findings implicate the four nuclear lamin isoforms as key determinants of whole-cell mechanics. We show that the loss of A-type lamins compromises cortical and cytoplasmic stiffness as well as cellular contractility, while the lack of B-type lamins affects cytoplasmic stiffness and cellular contractility but not cortical stiffness. These distinct mechanical changes correlate with the selective interactions of the A- and B-type lamins with LINC complexes containing nesprin-2G and/or nesprin-3 α , which physically couple the nucleus to the actomyosin and VIF cytoskeletons, respectively. Further in-depth studies are required to explore whether the loss of lamins or LINC complexes directly affects cell mechanics or whether indirect mechanism(s), such as

changes in chromatin organization and consequently cytoskeletal gene expression profiles, are also involved. We further demonstrate that the loss of each lamin isoform reduces heterochromatin levels, softens the nucleus, and promotes cell migration in constricted microenvironments resulting in significantly increased levels of double-stranded DNA damage. These insights expand our understanding of several fundamental nuclear lamina-dependent cellular processes, such as mechanotransduction and cell migration. Furthermore, they put forth potential underlying mechanism(s) for pathological cellular mechanophenotypes associated with mutations in lamins or changes in lamin isoform levels in diseases like laminopathies (e.g., dilated cardiomyopathy, muscular dystrophy, and the accelerated aging disorder Hutchinson–Gilford progeria syndrome) as well as a large number of cancers (74–76).

Materials and Methods

See *SI Appendix* for full description of the Materials and Methods.

Data Availability. All study data are included in the article and/or *SI Appendix*. Original data for AFM measurements, cell cycle analyses, and western blots have been deposited to the Northwestern University Arch data repository <https://arch.library.northwestern.edu> (<https://arch.library.northwestern.edu/concern/datasets/vq27zn830>).

ACKNOWLEDGMENTS. We thank Daniel Starr for the nesprin-3 antibody, Kyle Roux for the GFP-KASH4 construct, Arnoud Sonnenberg for EGFP-nesprin-3 α , David Kirchenbuechler for Imaris training and assistance with imaging data

analysis, Christopher Mauer for FRAP training, and Andrew Stephens for insightful discussions and critical review of the manuscript. This work made use of the SPID facility of Northwestern University's NUANCE Center, which has received support from the SHyNE Resource (NSF ECCS-2025633), the IIN, and Northwestern University's MRSEC program (NSF DMR-1720139). The imaging analysis with Imaris was performed at the Northwestern University Center for Advanced Microscopy, generously supported by NCI CCSG P30 CA060553, awarded to the Robert H. Lurie Comprehensive Cancer Center. This work was supported by the Northwestern University RHLCCC Flow Cytometry Facility and a Cancer Center Support Grant (NCI CA060553). This work was supported by NIH P01GM096971 (to R.D.G.), NIH R01GM106023 (to Y.Z. and R.D.G.), NIH R01GM140108 (to M.G. and R.D.G.), NIH R01HL148152 (to J.J.F.), NIH R01AG064944 and R35GM12858593 (to G.G.G.), NIH R01GM132427 (to K.L.R.), NIH R01GM129374 (to G.W.G.L.), and NIH 1K99EY032547-01 (to A.V.).

Author affiliations: ^aDepartment of Cell and Developmental Biology, Feinberg School of Medicine, Northwestern University, Chicago, IL 60611; ^bDepartment of Mechanical Engineering, Massachusetts Institute of Technology, Cambridge, MA 02139; ^cHarvard T. H. Chan School of Public Health, Harvard University, Boston, MA 02115; ^dHMMI, Janelia Research Campus, Ashburn, VA 20147; ^eRegenerative and Developmental Biology Group, Institute of Medical Biology, Singapore 138648; ^fDepartment of Embryology, Carnegie Institution for Science, Baltimore, MD 21218; ^gDepartment of Pathology and Cell Biology, Columbia University, New York, NY 10032; ^hDepartment of Biological Chemistry, Johns Hopkins University, Baltimore, MD 21205; and ⁱDepartment of Molecular and Cellular Biology, University of California, Davis, CA 95616

Author contributions: A.V., S.S., J.R.T., G.G.G., G.W.G.L., M.G., J.J.F., Y.Z., S.A.A., and R.D.G. designed research; A.V., S.S., F.A.S.N., Y.L.H., C.Y.P., and M.K. performed research; M.K., X.W., J.R.T., G.G.G., K.L.R., and G.W.G.L. contributed new reagents/analytic tools; A.V., S.S., F.A.S.N., Y.L.H., C.Y.P., M.K., K.L.R., M.G., J.J.F., Y.Z., and S.A.A. analyzed data; and A.V., S.S., Y.L.H., C.Y.P., M.K., K.L.R., G.W.G.L., M.G., J.J.F., Y.Z., S.A.A., and R.D.G. wrote the paper.

- D. M. Graham *et al.*, Enucleated cells reveal differential roles of the nucleus in cell migration, polarity, and mechanotransduction. *J. Cell Biol.* **217**, 895–914 (2018).
- A. J. Lomakin *et al.*, The nucleus acts as a ruler tailoring cell responses to spatial constraints. *Science* **370**, eaba2894 (2020).
- S. A. Adam, The nucleoskeleton. *Cold Spring Harb. Perspect. Biol.* **9**, a023556 (2017).
- T. Shimi *et al.*, Structural organization of nuclear lamins A, C, B1, and B2 revealed by superresolution microscopy. *Mol. Biol. Cell* **26**, 4075–4086 (2015).
- T. J. Kirby, J. Lammerding, Emerging views of the nucleus as a cellular mechanosensor. *Nat. Cell Biol.* **20**, 373–381 (2018).
- J. S. Lee *et al.*, Nuclear lamin A/C deficiency induces defects in cell mechanics, polarization, and migration. *Biophys. J.* **93**, 2542–2552 (2007).
- J. L. Broers *et al.*, Decreased mechanical stiffness in LMNA^{-/-} cells is caused by defective nucleocytoskeletal integrity: Implications for the development of laminopathies. *Hum. Mol. Genet.* **13**, 2567–2580 (2004).
- J. Lammerding *et al.*, Lamin A/C deficiency causes defective nuclear mechanics and mechanotransduction. *J. Clin. Invest.* **113**, 370–378 (2004).
- M. Guo *et al.*, Cell volume change through water efflux impacts cell stiffness and stem cell fate. *Proc. Natl. Acad. Sci. U.S.A.* **114**, E8618–E8627 (2017).
- S. Y. Tee, J. Fu, C. S. Chen, P. A. Janmey, Cell shape and substrate rigidity both regulate cell stiffness. *Biophys. J.* **100**, L25–L27 (2011).
- A. Agrawal, T. P. Lele, Geometry of the nuclear envelope determines its flexural stiffness. *Mol. Biol. Cell* **31**, 1815–1821 (2020).
- Y. Guo, Y. Zheng, Lamins position the nuclear pores and centrosomes by modulating dynein. *Mol. Biol. Cell* **26**, 3379–3389 (2015).
- R. D. González-Cruz, K. N. Dahl, E. M. Darling, The emerging role of lamin C as an important LMNA isoform in mechanophenotype. *Front. Cell Dev. Biol.* **6**, 151 (2018).
- R. D. González-Cruz, J. S. Sadick, V. C. Fonseca, E. M. Darling, Nuclear lamin protein C is linked to lineage-specific, whole-cell mechanical properties. *Cell. Mol. Bioeng.* **11**, 131–142 (2018).
- X. Wong *et al.*, Lamin C is required to establish genome organization after mitosis. *Genome Biol.* **22**, 305 (2021).
- K. E. Kasza *et al.*, Filamin A is essential for active cell stiffening but not passive stiffening under external force. *Biophys. J.* **96**, 4326–4335 (2009).
- G. Jovtchev, V. Schubert, A. Meister, M. Barow, I. Schubert, Nuclear DNA content and nuclear and cell volume are positively correlated in angiosperms. *Cytogenet. Genome Res.* **114**, 77–82 (2006).
- A. E. Patteson *et al.*, Vimentin protects cells against nuclear rupture and DNA damage during migration. *J. Cell Biol.* **218**, 4079–4092 (2019).
- M. D. Huber, L. Gerace, The size-wise nucleus: Nuclear volume control in eukaryotes. *J. Cell Biol.* **179**, 583–584 (2007).
- A. Vahabikashi *et al.*, Probe sensitivity to cortical versus intracellular cytoskeletal network stiffness. *Biophys. J.* **116**, 518–529 (2019).
- J. Hu *et al.*, High stretchability, strength, and toughness of living cells enabled by hyperelastic vimentin intermediate filaments. *Proc. Natl. Acad. Sci. U.S.A.* **116**, 17175–17180 (2019).
- K. Haase, A. E. Pelling, The role of the actin cortex in maintaining cell shape. *Commun. Integr. Biol.* **6**, e26714 (2013).
- P. Chugh, E. K. Paluch, The actin cortex at a glance. *J. Cell Sci.* **131**, jcs186254 (2018).
- J. P. Butler, I. M. Tolić-Nørrelykke, B. Fabry, J. J. Fredberg, Traction fields, moments, and strain energy that cells exert on their surroundings. *Am. J. Physiol. Cell Physiol.* **282**, C595–C605 (2002).
- M. Guo *et al.*, The role of vimentin intermediate filaments in cortical and cytoplasmic mechanics. *Biophys. J.* **105**, 1562–1568 (2013).
- G. Salbreux, G. Charras, E. Paluch, Actin cortex mechanics and cellular morphogenesis. *Trends Cell Biol.* **22**, 536–545 (2012).
- G. W. G. Luxton, E. R. Gomes, E. S. Folker, E. Vintinner, G. G. Gundersen, Linear arrays of nuclear envelope proteins harness retrograde actin flow for nuclear movement. *Science* **329**, 956–959 (2010).
- M. Ketema, M. Kref, P. Secades, H. Janssen, A. Sonnenberg, Nesprin-3 connects plectin and vimentin to the nuclear envelope of Sertoli cells but is not required for Sertoli cell function in spermatogenesis. *Mol. Biol. Cell* **24**, 2454–2466 (2013).
- Y.-Y. Zhen, T. Libotte, M. Munck, A. A. Noegel, E. Korenbaum, NUANCE, a giant protein connecting the nucleus and actin cytoskeleton. *J. Cell Sci.* **115**, 3207–3222 (2002).
- K. Wilhelmssen *et al.*, Nesprin-3, a novel outer nuclear membrane protein, associates with the cytoskeletal linker protein plectin. *J. Cell Biol.* **171**, 799–810 (2005).
- M. Ketema *et al.*, Requirements for the localization of nesprin-3 at the nuclear envelope and its interaction with plectin. *J. Cell Sci.* **120**, 3384–3394 (2007).
- V. C. Padmakumar *et al.*, The inner nuclear membrane protein Sun1 mediates the anchorage of Nesprin-2 to the nuclear envelope. *J. Cell Sci.* **118**, 3419–3430 (2005).
- M. Crisp *et al.*, Coupling of the nucleus and cytoplasm: Role of the LINC complex. *J. Cell Biol.* **172**, 41–53 (2006).
- C. Ostlund *et al.*, Dynamics and molecular interactions of linker of nucleoskeleton and cytoskeleton (LINC) complex proteins. *J. Cell Sci.* **122**, 4099–4108 (2009).
- E. S. Folker, C. Ostlund, G. W. Luxton, H. J. Worman, G. G. Gundersen, Lamin A variants that cause striated muscle disease are defective in anchoring transmembrane actin-associated nuclear lines for nuclear movement. *Proc. Natl. Acad. Sci. U.S.A.* **108**, 131–136 (2011).
- W. Chang *et al.*, Imbalanced nucleocytoskeletal connections create common polarity defects in progeria and physiological aging. *Proc. Natl. Acad. Sci. U.S.A.* **116**, 3578–3583 (2019).
- J.-K. Kim *et al.*, Nuclear lamin A/C harnesses the perinuclear apical actin cables to protect nuclear morphology. *Nat. Commun.* **8**, 2123 (2017).
- D. H. Kim, A. B. Chambliss, D. Wirtz, The multi-faceted role of the actin cap in cellular mechanosensation and mechanotransduction. *Soft Matter* **9**, 5516–5523 (2013).
- H. Wu *et al.*, Vimentin intermediate filaments and filamentous actin form unexpected interpenetrating networks that redefine the cell cortex. *Proc. Natl. Acad. Sci. U.S.A.* **119**, e2115217119 (2022).
- M. L. Lombardi *et al.*, The interaction between nesprins and sun proteins at the nuclear envelope is critical for force transmission between the nucleus and cytoskeleton. *J. Biol. Chem.* **286**, 26743–26753 (2011).
- D. Razařsky, D. Hodzic, Temporal and tissue-specific disruption of LINC complexes in vivo. *Genesis* **52**, 359–365 (2014).
- S. Neelam *et al.*, Direct force probe reveals the mechanics of nuclear homeostasis in the mammalian cell. *Proc. Natl. Acad. Sci. U.S.A.* **112**, 5720–5725 (2015).
- A. D. Stephens, E. J. Banigan, S. A. Adam, R. D. Goldman, J. F. Marko, Chromatin and lamin A determine two different mechanical response regimes of the cell nucleus. *Mol. Biol. Cell* **28**, 1984–1996 (2017).
- A. D. Stephens *et al.*, Chromatin histone modifications and rigidity affect nuclear morphology independent of lamins. *Mol. Biol. Cell* **29**, 220–233 (2018).
- O. Wintner *et al.*, A unified linear viscoelastic model of the cell nucleus defines the mechanical contributions of lamins and chromatin. *Adv. Sci. (Wein.)* **7**, 1901222 (2020).
- K. T. Sapra *et al.*, Nonlinear mechanics of lamin filaments and the meshwork topology build an emergent nuclear lamina. *Nat. Commun.* **11**, 6205 (2020).
- J. Swift *et al.*, Nuclear lamin-A scales with tissue stiffness and enhances matrix-directed differentiation. *Science* **341**, 1240104 (2013).

48. G. Tang, M. Galluzzi, B. Zhang, Y. L. Shen, F. J. Stadler, Biomechanical heterogeneity of living cells: Comparison between atomic force microscopy and finite element simulation. *Langmuir* **35**, 7578–7587 (2019).
49. C. M. Hobson *et al.*, Correlating nuclear morphology and external force with combined atomic force microscopy and light sheet imaging separates roles of chromatin and lamin A/C in nuclear mechanics. *Mol. Biol. Cell* **31**, 1788–1801 (2020).
50. X. Wang *et al.*, Intracellular manipulation and measurement with multipole magnetic tweezers. *Sci. Robot.* **4**, eaav6180 (2019).
51. M. M. Nava *et al.*, Heterochromatin-driven nuclear softening protects the genome against mechanical stress-induced damage. *Cell* **181**, 800–817.e22 (2020).
52. T. Harada *et al.*, Nuclear lamin stiffness is a barrier to 3D migration, but softness can limit survival. *J. Cell Biol.* **204**, 669–682 (2014).
53. J. R. Tran, X. Zheng, Y. Zheng, Lamin-B1 contributes to the proper timing of epicardial cell migration and function during embryonic heart development. *Mol. Biol. Cell* **27**, 3956–3963 (2016).
54. C. Coffinier *et al.*, Deficiencies in lamin B1 and lamin B2 cause neurodevelopmental defects and distinct nuclear shape abnormalities in neurons. *Mol. Biol. Cell* **22**, 4683–4693 (2011).
55. P. M. Davidson, C. Denais, M. C. Bakshi, J. Lammerding, Nuclear deformability constitutes a rate-limiting step during cell migration in 3-D environments. *Cell. Mol. Bioeng.* **7**, 293–306 (2014).
56. C. R. Pfeifer *et al.*, Constricted migration increases DNA damage and independently represses cell cycle. *Mol. Biol. Cell* **29**, 1948–1962 (2018).
57. M. Raab *et al.*, ESCRT III repairs nuclear envelope ruptures during cell migration to limit DNA damage and cell death. *Science* **352**, 359–362 (2016).
58. P. Shah *et al.*, Nuclear deformation causes DNA damage by increasing replication stress. *Curr. Biol.* **31**, 753–765.e6 (2021).
59. L. J. Kuo, L. X. Yang, Gamma-H2AX—A novel biomarker for DNA double-strand breaks. *In Vivo* **22**, 305–309 (2008).
60. R. Vargas-Pinto, H. Gong, A. Vahabikashi, M. Johnson, The effect of the endothelial cell cortex on atomic force microscopy measurements. *Biophys. J.* **105**, 300–309 (2013).
61. A. E. Patteson, A. Vahabikashi, R. D. Goldman, P. A. Janmey, Mechanical and non-mechanical functions of filamentous and non-filamentous vimentin. *BioEssays* **42**, e2000078 (2020).
62. O. Wiggan, J. G. DeLuca, T. J. Stasevich, J. R. Bamberg, Lamin A/C deficiency enables increased myosin-II bipolar filament ensembles that promote divergent actomyosin network anomalies through self-organization. *Mol. Biol. Cell* **31**, 2363–2378 (2020).
63. M. Kittisopikul *et al.*, Computational analyses reveal spatial relationships between nuclear pore complexes and specific lamins. *J. Cell Biol.* **220**, e202007082 (2021).
64. F. Alisafaei, D. S. Jokhun, G. V. Shivashankar, V. B. Shenoy, Regulation of nuclear architecture, mechanics, and nucleocytoplasmic shuttling of epigenetic factors by cell geometric constraints. *Proc. Natl. Acad. Sci. U.S.A.* **116**, 13200–13209 (2019).
65. Y. Jiu *et al.*, Bidirectional interplay between vimentin intermediate filaments and contractile actin stress fibers. *Cell Rep.* **11**, 1511–1518 (2015).
66. Y. Shen *et al.*, Effects of vimentin intermediate filaments on the structure and dynamics of in vitro multicomponent interpenetrating cytoskeletal networks. *Phys. Rev. Lett.* **127**, 108101 (2021).
67. N. Costigliola *et al.*, Vimentin fibers orient traction stress. *Proc. Natl. Acad. Sci. U.S.A.* **114**, 5195–5200 (2017).
68. D. Tsuruta, J. C. Jones, The vimentin cytoskeleton regulates focal contact size and adhesion of endothelial cells subjected to shear stress. *J. Cell Sci.* **116**, 4977–4984 (2003).
69. M. G. Mendez, S. Kojima, R. D. Goldman, Vimentin induces changes in cell shape, motility, and adhesion during the epithelial to mesenchymal transition. *FASEB J.* **24**, 1838–1851 (2010).
70. J. Lammerding *et al.*, Lamins A and C but not lamin B1 regulate nuclear mechanics. *J. Biol. Chem.* **281**, 25768–25780 (2006).
71. M. Vortmeyer-Krause *et al.*, Lamin B2 follows lamin A/C-mediated nuclear mechanics and cancer cell invasion efficacy. *bioRxiv* [Preprint] (2020). <https://doi.org/10.1101/2020.04.07.028969>.
72. K. Wolf *et al.*, Physical limits of cell migration: Control by ECM space and nuclear deformation and tuning by proteolysis and traction force. *J. Cell Biol.* **201**, 1069–1084 (2013).
73. C. R. Pfeifer, M. Vashisth, Y. Xia, D. E. Discher, Nuclear failure, DNA damage, and cell cycle disruption after migration through small pores: A brief review. *Essays Biochem.* **63**, 569–577 (2019).
74. M. Maurer, J. Lammerding, The driving force: Nuclear mechanotransduction in cellular function, fate, and disease. *Annu. Rev. Biomed. Eng.* **21**, 443–468 (2019).
75. D. E. Discher *et al.*, Matrix mechanosensing: From scaling concepts in 'omics data to mechanisms in the nucleus, regeneration, and cancer. *Annu. Rev. Biophys.* **46**, 295–315 (2017).
76. C. R. Pfeifer, C. M. Alvey, J. Irianto, D. E. Discher, Genome variation across cancers scales with tissue stiffness—An invasion-mutation mechanism and implications for immune cell infiltration. *Curr. Opin. Syst. Biol.* **2**, 103–114 (2017).